Quantum dynamics of adsorbed H_2 in the microporous framework MOF-5 analyzed using diffuse reflectance infrared spectroscopy

S. A. FitzGerald, K. Allen, P. Landerman, J. Hopkins, J. Matters, and R. Myers
Department of Physics and Astronomy, Oberlin College, Oberlin, Ohio 44074, USA

J. L. C. Rowsell
Department of Chemistry and Biochemistry, Oberlin College, Oberlin, Ohio 44074, USA
(Received 6 February 2008; published 5 June 2008)

Diffuse reflectance infrared spectroscopy is used to measure the quantum dynamics of molecular hydrogen adsorbed in the microporous material MOF-5. Low-temperature spectra reveal at least three distinct binding sites. The induced redshifts in the vibrational mode frequencies allow the estimation of site-specific binding energies ranging from 2.5 to 4 kJ/mol. Splittings in the rovibrational sidebands are consistent with the existing theories and indicate that H_2 is relatively freely rotating even at temperatures as low as 10 K. *Ortho* to *para* conversion of the adsorbed H_2 is observed to occur over the course of several hours. A translational sideband of 84 cm^{-1} arises from the center-of-mass motion of H_2 at the primary adsorption site and indicates that the zero-point energy is a substantial fraction of the binding energy of this site.

DOI: 10.1103/PhysRevB.77.224301 PACS number(s): 78.30.−j, 82.75.−z

I. INTRODUCTION

While formidable technical challenges remain for the efficient, clean generation and conversion of hydrogen, no technology exists that fulfills the criteria for storing this energy carrier within its most important proposed consumer: the automobile.[1] Consequently, chemical and physical adsorbents have been intensely explored to increase the gravimetric and volumetric capacities of storage devices, operating at near-ambient conditions. Among the best physisorbents—those that bind hydrogen in molecular form to the internal surfaces of pores through dispersion forces—are several microporous metal carboxylates, members of a group of materials known as coordination polymers or metal-organic frameworks (MOFs).[2,3] Gravimetric hydrogen adsorption capacities of approximately 7 wt % have been demonstrated at 77 K,[4,5] and although this achievement is far from the targeted *system* (adsorbent plus container, gauges, and accessories) storage capacity of 9 wt % at ambient temperature,[6] the myriad of structure types discovered in the past decade provides some optimism that a future material will meet the requirements. In the meantime, MOFs provide ideal subjects for the development of experimental and theoretical tools to expand our understanding of hydrogen adsorption.

The *catena*-tris(μ_4-benzene-1,4-dicarboxylato)-μ_4-oxo-tetrazinc(II) material known as MOF-5[7] and IRMOF-1[8] is an excellent model physisorbent for several reasons. For experimentalists, samples of the material are easily prepared by a scalable solvothermal synthesis requiring no specialized equipment. Crystal growth conditions can be adjusted to vary the average particle size, and samples consisting of well-formed crystals allow purity determination by powder x-ray diffraction and optical microscopy. For theoreticians, the high-symmetry disorder-free periodic structure of the material simplifies data interpretation and lends itself to more advanced computational simulations with fewer assumptions. Most importantly, the material is very microporous (voids 1.2 and 1.5 nm in diameter account for nearly 80% of the crystalline volume) and demonstrates exceptional adsorption behavior, including a gravimetric H_2 capacity of ~5 wt % at 77 K.[9–12]

Given these attributes, a detailed understanding of hydrogen physisorption by MOF-5 is the motivation behind several recent reports. Among these studies, neutron diffraction has provided the most descriptive experimental evidence of the preferred H_2 adsorption sites in this material.[13,14] Below 50 K, there is evidence of H_2 localization in the corners of the 1.5 nm pores on the alternate faces of the inorganic $Zn_4O(O_2C-)_6$ clusters. At lower temperatures and higher loadings, secondary sites are occupied, first around the inorganic clusters, and then on the phenylene links. This behavior is analogous to that previously modeled for nitrogen and argon by x-ray diffraction analyses.[15] While these seemingly static depictions of the periodic locations of H_2 in the crystalline adsorbent have provided invaluable structural information, it is important to recognize that they represent long temporal and spatial averages of adsorbate behavior that is known to be dynamic even at very low temperatures. Moreover, diffraction techniques have not yet been shown to provide information about the energetics of these interactions, except in a relative sense by comparing fractional site occupations as a function of temperature and adsorptive loading. Information about the preferential occupation of discrete surface sites is useful for evaluating theoretical models aimed at estimating the magnitude of these interactions.[16–24]

Inelastic neutron scattering (INS) spectroscopy is a powerful technique for studying the energetics of rotational transitions and it has already been used to characterize the localized H_2 adsorption sites in MOF-5 and related zinc carboxylates.[25] The advantages of this technique arise from the uniquely large neutron scattering cross section of ^1H and the ability of neutrons to induce nuclear spin transitions, thereby allowing observation of the rotational $\Delta J=1$ (i.e., *ortho* to *para*) transitions that would otherwise be forbidden.[26] Hydrogen molecules experience a potential barrier to rotation when adsorbed, altering the degeneracy and

spacing of energy levels.[27] Consequently, INS spectra are rich in information about the chemical environments of adsorbed H_2; however, the limited energy resolution and restricted beam time for experiments present practical challenges for investigating this behavior on a site-by-site basis. Mid-infrared photons provide a complementary source of insight, revealing both the vibrational, rotational-vibrational, and center-of-mass transitions of adsorbed molecules. Activation of H_2 infrared (IR) modes results from interactions with the framework atoms, producing weak—yet observable—spectral features that are specific to the chemical nature of the adsorption site.[28] Propitiously, an interpretation of these features only concerns adsorbed molecules, as gas phase (nonperturbed) H_2 are infrared inactive.

In this study, diffuse reflectance IR spectroscopy is employed to observe the dynamics of adsorbed H_2 in MOF-5 at low temperatures. This geometry greatly enhances the optical absorption strength of a sample, allowing us to overcome challenges related to the weak IR activity of adsorbed H_2.[29] New information is gleaned about the center-of-mass dynamics, degree of anisotropy, and adsorption energy associated with the primary adsorption site. In addition, we observe the occupation of secondary sites at larger H_2 concentrations. The time-dependent nature of the spectra is also used to monitor the *ortho* to *para* conversion of the adsorbed H_2. These observations should prove crucial in the refinement of physisorption models as researchers continue to search for materials with larger affinities for hydrogen.

II. THEORY

Gas phase H_2 vibrates at a frequency of 4161 cm^{-1} and acts as a near perfect quantum rotor with rotational energy levels,

$$E(J) = B_v J(J+1), \tag{1}$$

where J is the rotational quantum number and B is the rotational constant, having values of 59 cm^{-1} in the ground vibrational state and 56 cm^{-1} in the first excited vibrational state.[30] Quantum statistics constrain the total molecular wave function to be odd under nuclear exchange. As such, H_2 molecules with total nuclear spin, $I=1$ (*ortho*-hydrogen), must have an odd J quantum number, while those with $I=0$ (*para*-hydrogen) must have an even J. The only way to convert between *ortho*- and *para*-hydrogen is to "flip" a nuclear spin; thus photon-induced transitions are limited to cases in which $\Delta J=0$ or $\Delta J=\pm 2$.[31]

In the mid-IR region, we are probing excitations in which H_2 undergoes a vibrational transition. If $\Delta J=0$, then these transitions are purely vibrational and referred to as Q transitions. If $\Delta J=+2$, then the H_2 also undergoes an excitation of its rotational state (rovibrational transition) and it is referred to as an S transition. The transition frequencies for gas phase hydrogen are shown in Fig. 1. In the absence of *ortho* to *para* conversion, there are four possible transitions at low temperature: the pure vibrational $Q(0)$ and $Q(1)$, which differ by only 6 cm^{-1}, and the rovibrational transitions $S(0)$ and $S(1)$. The number in parentheses refers to the J value of the initial state.

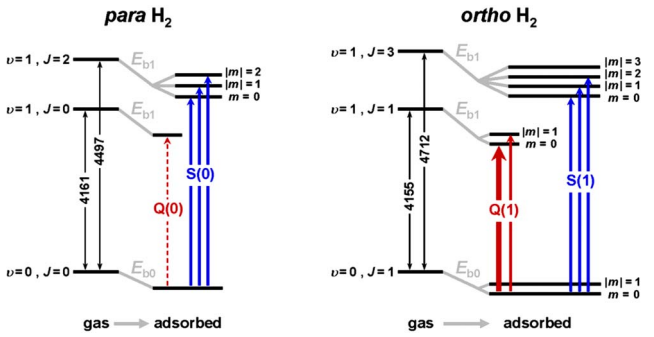

FIG. 1. (Color online) Energy level diagram (not to scale) showing the rotational-vibrational transitions for H_2 in a perturbing host, where v is the vibrational quantum number and J is the rotational quantum number. The scheme is modeled after the primary binding site in MOF-5, for which the absolute value of m is still a good quantum number. The numbers show the gas phase transition frequencies in cm^{-1}. E_{b0} and E_{b1} are the binding energies in the ground and excited vibrational states, respectively. The solid arrows show transitions activated by the quadrupolar mechanism, while the dashed arrow indicates a transition activated by the isotropic mechanism [$Q(0)$]. The $Q(1)$ transition with $\Delta m=0$ (thick arrow) is activated by both mechanisms.

Infrared transitions can only occur (fundamentally) if the transition leads to a change in the dipole moment of the system (i.e., H_2 *and* framework).[32] As a homonuclear diatomic molecule, H_2 has no dipole moment and therefore no intrinsic IR activity. The observed absorption spectrum arises through the presence of interaction-induced dipole moments between H_2 and the neighboring framework atoms.[33] There are two basic mechanisms by which this occurs. In the first, the framework atoms interact with the H_2 polarizability to induce a dipole moment on the molecule; because the H_2 polarizability is essentially isotropic, to a good approximation, this mechanism only activates Q transitions and not those involving a change in the H_2 rotational state, i.e., $S(0)$ or $S(1)$.[34] Herein, we refer to this as the *isotropic* mechanism. The second method of IR activation involves the H_2 permanent quadrupole moment, inducing an interaction dipole moment on the framework atoms, and is therefore denoted as the *quadrupole* mechanism. A transition to a new H_2 state leads to a change in both its quadrupole moment and the dipole it induces on the framework atoms, thus meeting the requirement for IR activity. In contrast to its polarizability, the H_2 quadrupole moment is highly anisotropic and this term leads to the activation of rovibrational $S(0)$ and $S(1)$ transitions in addition to $Q(1)$. In contrast, $Q(0)$ transitions are not activated because the $J=0$ state is spherically symmetric and possesses no quadrupole moment.[35] These guidelines are summarized in Fig. 1. The isotropic mechanism, which dominates at short range, leads to $Q(0)$ and $Q(1)$ (with $\Delta m=0$) transitions. The quadrupole mechanism, which dominates for long-range interactions and in cases where the binding site is surrounded by framework species with large polarizabilities, activates $Q(1)$, $S(0)$, and $S(1)$ transitions.

In addition to making the transitions IR active, interactions with the framework also lead to a splitting and frequency shift of the modes relative to the gas phase. The

frequency shift is primarily associated with the anharmonicity in the H_2 vibrational motion, leading to an increased H—H bond length, which in turn changes the interaction energy with the framework.[28] As illustrated in Fig. 1, this interaction is typically stronger for H_2 in its vibrationally excited state than in its ground state, yielding a positive relationship between the interaction energy and the redshift of the vibrational mode.[36]

Framework interactions also remove the degeneracy of the H_2 rotational levels. Traditionally, this can be understood by expanding the interaction potential in terms of spherical harmonics,[37]

$$V(\theta,\phi) = V_0 + \sum_{L=1}^{\infty} \sum_{m=-L}^{m=L} A_L^m Y_L^m(\theta,\phi), \tag{2}$$

where θ and ϕ are the spherical polar coordinates representing the orientation of H_2, and V_0 is the isotropic part of the potential that determines the interaction energy and is generally much larger than the anisotropic terms. The resultant degeneracy of the different J rotational levels is determined by the symmetry of the particular H_2 binding site. Experimentally, this is manifested by the number of bands in the $S(0)$ and $S(1)$ regions. The frequency separation of these bands provides quantitative information about the anisotropy of the orientational potential and, in particular, the barrier to free rotation. This is similar to the information gleaned by INS spectroscopy.

III. EXPERIMENTAL SECTION

Samples of crystalline, high-purity $Zn_4O(C_8H_4O_4)_3$ (MOF-5) were prepared by using an established solvothermal synthesis, employing N,N-diethylformamide as the solvent.[9] Benzene-1,4-dicarboxylic acid (0.75 g, 4.5 mmol, Aldrich) and zinc nitrate tetrahydrate (3.0 g, 11 mmol, EM Science) were dissolved in 100 ml of N,N-diethylformamide (TCI, decolorized with activated carbon and further purified by flash chromatography through a silica gel column prior to use) with stirring in a 1 l wide mouth glass jar. The jar was tightly capped and placed in a 90 °C oven for 24 h to yield cubic crystals. After decanting the hot mother liquor and rinsing with N,N-dimethylformamide (Fisher), the product was immersed in chloroform (Fisher) for 3 days, during which the activation solvent was decanted and freshly replenished three times. The solvent was removed under vacuum at room temperature, yielding the porous material. The deuterated analog of this material, $Zn_4O(C_8D_4O_4)_3$, was readily prepared by substituting ring-d_4-benzene-1,4-dicarboxylic acid (Cambridge Isotopes, 98% enrichment) for the organic acid in the reaction solution.

The bulk purity of the MOF-5 samples was confirmed by optical microscopy, powder x-ray diffraction (PXRD), elemental analysis, and gas adsorption measurements. Under the above-described synthetic conditions, the material forms as predominantly single crystals approximately 0.3 mm in dimension. No evidence of noncubic or amorphous phases was observed by optical microscopy. Aliquots were lightly ground and analyzed by PXRD (Philips X'Pert MPD-3040 diffractometer), yielding the same diffraction patterns as those calculated from previously reported structural data.[9,13,15] The compositions of the samples were determined by elemental analyses (Atlantic Microlab): for $Zn_4O(C_8H_4O_4)_3$ (% calc./found), C, 37.4/37.4; H, 1.57/1.58; N, 0/<0.3; and O, 27.0/26.9 and for $Zn_4O(C_8D_4O_4)_3$ (% calc./found), C, 36.9/36.7; D, 3.09/3.28; N, 0/<0.3; and O, 26.6/26.5. Finally, the large adsorption capacities of the samples were demonstrated by N_2, H_2, and D_2 volumetric adsorption measurements (Micromeritics ASAP 2010, 77 K, up to 1 atm), yielding isotherms and calculated surface areas and pore volumes comparable to those previously published.[9,38]

Spectroscopic analyses of molecular hydrogen adsorbed within the pores of MOF-5 were performed by using a custom-built diffuse reflectance system. The sample chamber allows both the temperature and the atmospheric environment of the material to be controlled, as detailed in a recent publication.[39] IR spectra were acquired by using a Bomem DA3 Michelson interferometer equipped with a globar source, CaF_2 beamsplitter, and a liquid nitrogen cooled mercury cadmium telluride detector. A resolution of 0.1 cm^{-1} was used for the data collection. The sample holder and diffuse reflectance optics (Spectra-Tech Collector II) were mounted within a large vacuum chamber equipped with CaF_2 windows. Samples of MOF-5 (~10 mg) were transferred under inert atmosphere to a cup affixed to a copper slab, providing thermal contact to a cold-finger cryostat (Janis ST-300T). A custom-built high-pressure sapphire dome (Omley Ind.) was then affixed over the cup, such that hydrogen gas could be introduced to the sample through a high-pressure capillary soldered at the base of the cup. The sample was evacuated for several hours at room temperature prior to the introduction of hydrogen gas. Known volumes of research grade H_2 (99.9999%) were dispensed from a calibrated gas manifold by monitoring the change in pressure. The material and adsorbate were then equilibrated at 30–50 K for at least 10 min.

IV. RESULTS AND DISCUSSION

A. Sample characterization

We employed a modified version of the original synthesis procedure that uses N,N-diethylformamide (DEF) as the solvent, which has been independently shown to produce MOF-5 and related Zn_4O-based frameworks with expectedly large gas adsorption capacities.[8–11,40] The bulk purities of our samples were confirmed by optical microscopy, PXRD, elemental analysis, and adsorption measurements (N_2, H_2, and D_2). Analysis of the N_2 77 K adsorption isotherm measured for deuterated MOF-5 yielded an apparent Langmuir surface area of 3.8×10^3 m^2/g (by fitting 21 data in the range $0.006<P/P_0<0.64$), an apparent Brunauer-Emmett-Teller (BET) surface area of 3.3×10^3 m^2/g (8 data, $0.006<P/P_0<0.052$), and a Dubinin-Radushkevich-derived pore volume of 1.3 cm^3/g (11 data, $0.015<P/P_0<0.19$).[41] The linearity range used for the BET analysis was chosen according to the criteria that were discussed by Rouquerol *et al.*[42] The H_2 and D_2 isotherms (77 K, up to 1 bar) for this material

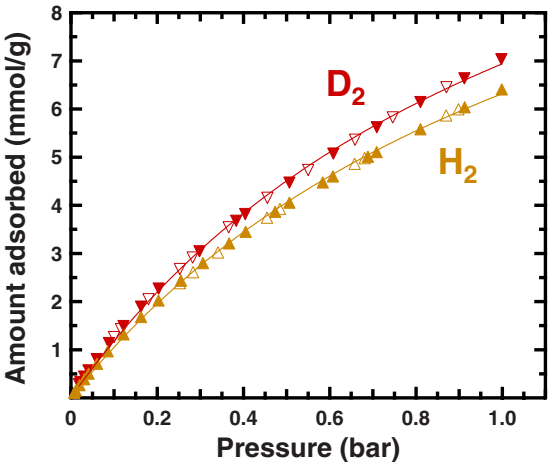

FIG. 2. (Color online) Adsorption isotherms for H_2 (▲) and D_2 (▼) in MOF-5 measured at 77 K. The closed symbols are adsorption data, the open symbols are desorption data, and the solid traces are Langmuir fits to the adsorption data.

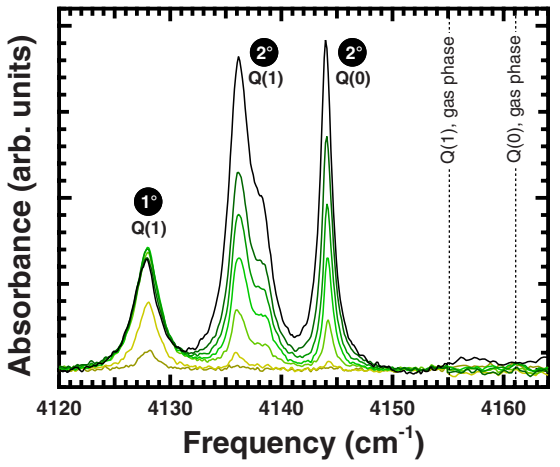

FIG. 3. (Color online) Diffuse reflectance spectra of adsorbed H_2 in MOF-5 at loadings of one, two, three, four, five, six, and eight molecules per $Zn_4O(O_2C–)_6$ cluster. The data were collected at 30 K. The band assignments are labeled according to their transition, $Q(0)$ or $Q(1)$, and corresponding adsorption site, primary (1°) or secondary (2°).

are shown in Fig. 2; the H_2 data are in excellent agreement with the independent measurements reported for MOF-5.[38,43] The D_2 isotherm shows an approximately 10% larger molar adsorption across the pressure range, which is similar to that observed for another MOF material, HKUST-1.[44] This increase arises from the smaller zero-point energy of adsorbed D_2 and is discussed in greater detail below, as it is pertinent to the spectroscopic analysis of the adsorbate center-of-mass motion.

A faster, less expensive MOF-5 synthesis involving the solvent *N*,*N*-dimethylformamide (DMF) has been proposed; however, this yields a less-porous material with a PXRD pattern that does not match that of MOF-5.[45] It was recently shown that this material consists of impure MOF-5 with occluded Zn complexes (that are presumably irremovable) as well as an interpenetrated form, both of which have significantly reduced pore volumes.[46] This information has an important bearing on a previous analysis of H_2 in MOF-5 by using IR spectroscopy,[47] which examined samples prepared by using the method of Huang *et al.*[45]

B. Vibrational spectroscopy

The diffuse reflectance geometry presents some important advantages for the acquisition of IR spectra of powdered substances. Materials are mounted in a sample cup without the need for further processing; in contrast, traditional transmission techniques require the powder to be pressed into an extremely thin pellet often with the aid of an inert binder and/or diluent, such as KBr. At the high frequency of the H_2 vibration, this latter protocol is plagued by scattering effects within the sample grains, leading to very low transmission.[29] Strong scattering is, in fact, beneficial for the diffuse reflectance technique because it leads to a longer optical path length within the sample. Incoming photons experience a range of optical path lengths, leading to an enhancement of weaker H_2 modes.[29,48]

As implied in Fig. 1, there are three spectral regions of interest, wherein H_2 vibrational and rovibrational transitions are expected: the Q region around 4160 cm^{-1}, $S(0)$ region near 4500 cm^{-1}, and the $S(1)$ region proximate to 4700 cm^{-1}. Bands shifted from the gas phase frequencies (indicated in Fig. 1) provide information about the adsorption energy and symmetry of the corresponding adsorption sites. To distinguish H_2 bound at different sites, the spectra measured at various loadings and temperatures are compared. Additional clues for aiding band assignments are provided by the slow *ortho* to *para* conversion that occurs in normal H_2 upon cooling. An increasing intensity at constant temperature and H_2 loading evinces a particular band that is associated with a $Q(0)$ or $S(0)$ transition, while $Q(1)$ and $S(1)$ bands diminish in intensity with time. Our observations of H_2 in MOF-5 suggest that this occurs at a rate of 25%/h.

Spectra containing bands assigned to Q transitions of adsorbed H_2 in MOF-5 are presented in Fig. 3. Individual spectra corresponding to H_2 loadings increasing from one to six molecules per $Zn_4O(O_2C–)_6$ cluster (0.26–1.6 wt %) are overlaid to illustrate the nonuniform population of the adsorption sites from which these features arise. At the smallest H_2 concentration, only a single Q band at 4128 cm^{-1} is observed. Its intensity increases with adsorbate loading until four H_2 per $Zn_4O(O_2C–)_6$ cluster, signifying the saturation of the corresponding adsorption site, which we denote as the primary (1°) site. The intensity of this band actually decreases following saturation, which is consistent with the progression of *ortho* to *para* conversion. At loadings greater than two H_2 per inorganic cluster, additional bands appear at 4144 cm^{-1} and 4136 cm^{-1}, with a shoulder at 4138 cm^{-1}. The shoulder displays unique concentration and temperature dependencies and is therefore associated with a different site than the 4136 cm^{-1} feature. Collectively, the adsorption sites that are responsible for these less-redshifted bands are referred to as the secondary (2°) sites. The designation of a band as a $Q(0)$ or $Q(1)$ transition is determined by observing its change in intensity due to *ortho* to *para* conversion over the course of a few hours. Interestingly, we do not observe a

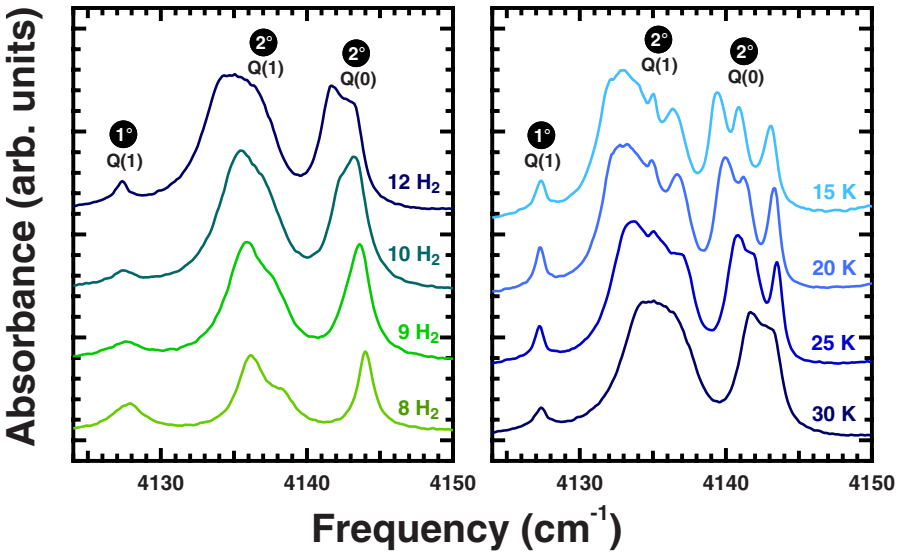

FIG. 4. (Color online) Left: Diffuse reflectance spectra of adsorbed H_2 in MOF-5 at loadings of 8–12 molecules per $Zn_4O(O_2C–)_6$ cluster. The data were collected at 30 K. Right: Spectra of the material loaded with 12 H_2 per $Zn_4O(O_2C–)_6$ cluster at temperatures between 15 and 30 K. The band assignments are labeled according to their transition, $Q(0)$ or $Q(1)$, and corresponding adsorption site, primary (1°) or secondary (2°). Spectra are vertically offset for clarity.

$Q(0)$ band arising from the primary site, which would be the case if the quadrupole mechanism is responsible for its IR activity.[35] The secondary site $Q(0)$ band has a full width at half maximum (FWHM) of 1 cm^{-1}, while the $Q(1)$ bands have a FWHM on the order of 2 cm^{-1}. The increased width of the $Q(1)$ bands is to be expected because the transition to a degenerate excited state leads to dephasing and relaxation effects.[49] Similarly, Xiao and Coker[50] predicted that transitions involving $J=1$ levels should have a maximum width due to the large anisotropy of the $J=1$ spherical harmonic wave function.

As explained in Sec. II, the majority of the Q bands are significantly redshifted relative to the corresponding gas phase value due to anharmonicity in the H_2 vibrational motion. As shown in Fig. 1, the adsorption energy is typically larger in magnitude for H_2 in the vibrationally excited state.[36] It is reasonable to associate the most redshifted band with the site of greatest adsorption energy; this is consistent with our results in Fig. 3, where the primary band that appears first upon loading also has the largest vibrational redshift (27 cm^{-1}). The observation that this band also saturates at four H_2 per inorganic cluster strongly suggests its correspondence to H_2, which occupies the primary binding site identified from diffraction studies, the so-called α or "cup" site.[13–15] Crystallographic symmetry dictates that this site has a maximum capacity of four H_2 per inorganic cluster, while secondary sites (β and γ) on the inorganic cluster can accommodate up to 16 more H_2 molecules. The secondary bands, with redshifts of 19 and 17 cm^{-1}, are tentatively assigned to the H_2 occupying these secondary sites; however, their overlap precludes an accurate determination of their saturation loadings. At larger concentrations, it is also possible for H_2 to occupy the sites on the organic links, and the features corresponding to these sites may also be overlapping in this region.

Figure 4 illustrates the evolution of the Q bands as the concentration of hydrogen is further increased; both broadening and redshifting are the general trends. In the case of the $Q(0)$ band originally at 4144 cm^{-1}, there is now clear evidence that it is composed of at least two distinct bands. Upon cooling the sample to 15 K, these bands show a continued systematic shift to lower frequency but now with a marked sharpening of the peaks. This allows the substructure to be quite clearly seen, and at 15 K, there are three bands with $Q(0)$ behavior along with their matching $Q(1)$ bands shifted by 6 cm^{-1} to lower frequency. The broadening and redshifting of the bands with increasing H_2 concentration are likely due to the $H_2\cdots H_2$ interactions between proximate adsorption sites. Cooling the sample to 15 K sharpened the bands and lead to a further redshift, which may be due to the increased H_2 adsorption rather than an intrinsic temperature effect. The secondary bands show frequency shifts on the order of 1–3 cm^{-1}, while the primary band shifts by less than 0.5 cm^{-1}. For comparison, in solid hydrogen wherein each H_2 is surrounded by 12 nearest neighbors, there is a 6 cm^{-1} redshift due to the $H_2\cdots H_2$ interactions with negligible temperature dependence.[34]

C. Center-of-mass translational mode

We observed two additional features in the Q region that are significantly blueshifted relative to the gas phase values. These are partially obscured by the overlapping bands arising from vibrational motion of the MOF-5 framework; therefore, a deuterated analog of this material was prepared and used for the analysis. These two materials are nearly identical in their physicochemical properties and all of the adsorbed H_2 bands appear in the same manner for deuterated MOF-5, but with less background interference in the 4150–4300 cm^{-1} region. Figure 5 highlights this region and the two features that are blueshifted relative to the gas phase frequencies. Both exhibit concentration dependencies associated with the primary adsorption site. Monitoring the behavior of these features revealed the sharp band at 4194 cm^{-1} to have a $Q(1)$ characteristic (decreasing intensity with time), while the broad feature is actually composed of a $Q(1)$ band at 4212 cm^{-1} and a $Q(0)$ band at 4217 cm^{-1}. The FWHM of these last two bands is ~4 cm^{-1}, which is significantly larger than that of all of the other Q bands. The blueshifted frequencies of these bands along with their larger FWHM

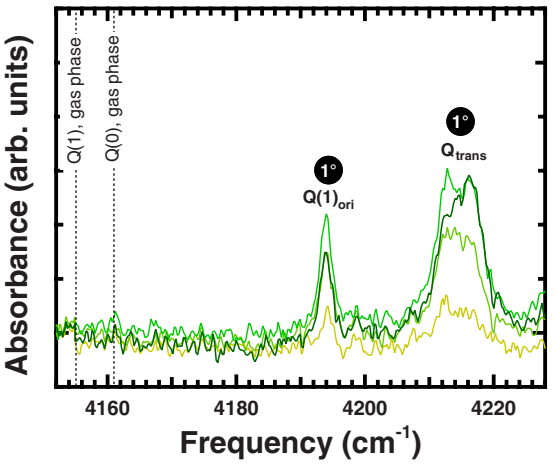

FIG. 5. (Color online) Diffuse reflectance spectra of adsorbed H_2 in MOF-5 at loadings of two, three, four, and six molecules per $Zn_4O(O_2C-)_6$ cluster. The data were collected at 30 K. $Q(1)_{ori}$ refers to a transition in which the H_2 also undergoes an orientational change with the m quantum number changing by ± 1. Q_{trans} refers to a transition in which the H_2 also undergoes a change in its center-of-mass translational state. 1° indicates that the H_2 is located in the primary site.

indicate that the latter features are associated with translational sidebands, in which the center-of-mass motion of the adsorbed H_2 undergoes a change in its quantum state. In general, translational sidebands are broader than the pure vibrational bands due to anisotropy and dephasing effects.[49,51] The $Q(1)$ band frequency of 4212 cm^{-1} is 84 cm^{-1} higher than that of the pure vibrational band, and thus, we can take the center-of-mass translational frequency to be 84 cm^{-1}. This is similar to that observed for H_2 in argon (112 cm^{-1}),[28] H_2 in C_{60} (110 cm^{-1}),[48,51] and most recently H_2 in a Cu based MOF, which is known as HKUST-1 (90 cm^{-1}).[52]

Approximating the center-of-mass translational motion as that of an isotropic three-dimensional simple harmonic oscillator yields a zero-point energy (ZPE) of $\frac{3}{2}\hbar\omega$, where ω is the center-of-mass translational frequency. From our translational band assignment in Fig. 5, a ZPE on the order of 1.5 kJ/mol is derived, which is a significant fraction of the total binding energy (2–7 kJ/mol) (Refs. 10, 11, 17, 19, 23, 24, 40, and 43) that is associated with the primary adsorption site and serves as a warning that quantum mechanical effects need to be included in any detailed theoretical modeling.

ZPE effects are most clearly observed in the differing behavior of adsorbed H_2 and D_2. The ZPE of an adsorbed D_2 molecule is reduced by a factor of $\sqrt{2}$ (in the harmonic approximation) relative to that of H_2; for the primary site, this corresponds to a ZPE of 1.1 kJ/mol. A simple Langmuir model predicts that this ZPE difference results in a 16% increase in the initial slope of the 77 K adsorption isotherm—which approximates Henry's law constant—for D_2 relative to H_2. This is similar to the observed increase of 12%, as shown in Fig. 2, especially considering the fact that there will be some population of secondary adsorption sites as well as some anharmonicity in the center-of-mass potential.

The remaining blueshifted feature in Fig. 5, which is denoted as $Q(1)_{ori}$, corresponds to an orientational transition involving a change in the rotational m quantum number. This is explained in further detail below, where we consider rotational transitions in general. The frequencies of all of the main Q features are listed in Table I.

TABLE I. Frequencies of the observed $Q(0)$, $Q(1)$, $S(0)$, and $S(1)$ transitions classified by binding site. Transition frequencies are in cm^{-1}.

Site	$Q(0)$	$Q(1)$	$S(0)$	$S(1)$
Gas	4161.2	4155.3	4497.8	4712.9
Primary		4127.8	4448.5	4676.1
		4194.0	4491	4712.1
	4217[a]	4212[a]		4734.5
Secondary	4144.2	4136.3	4461.1	4700
		4138.1	4470.5	
			4473.5	
			4490.4	

[a]Refers to center-of-mass translational bands.

D. Rovibrational bands

By using the diffuse reflection technique, several bands assignable to vibrational transitions involving a change in rotational quantum number are also observed. These rovibrational bands were not discerned in a previous study of H_2 in MOF-5 using transmission spectroscopy.[47] Figure 6 highlights the bands that appear in the $S(0)$ region as the concentration of hydrogen in the material is increased. Features at 4449 and 4491 cm^{-1} appear first and exhibit a similar saturation behavior as the primary bands observed in the Q region. Several weaker bands not associated with the primary site are also present at higher loading. As discussed above,

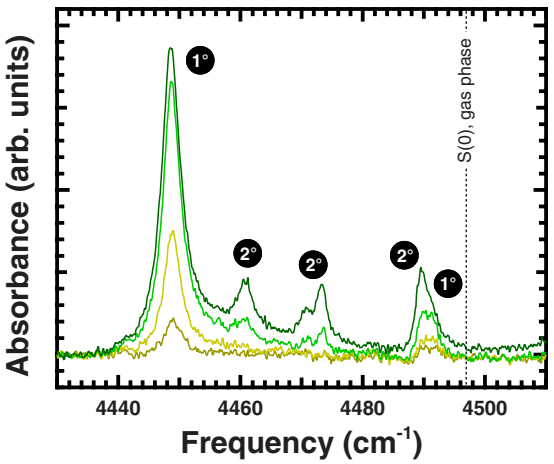

FIG. 6. (Color online) $S(0)$ transitions in the diffuse reflectance spectra of adsorbed H_2 in MOF-5 at loadings of one, two, four, and six molecules per $Zn_4O(O_2C-)_6$ cluster. The data were collected at 30 K. The band assignments are labeled according to their adsorption sites, primary (1°) or secondary (2°).

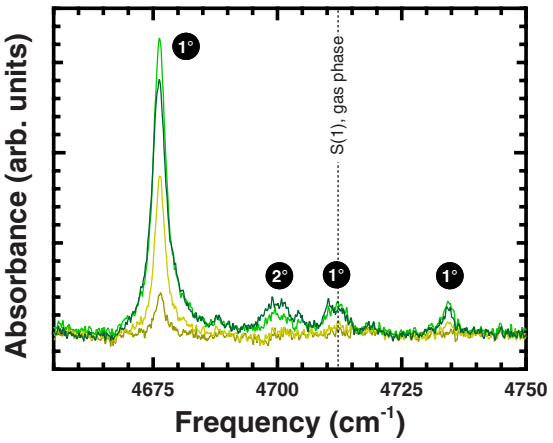

FIG. 7. (Color online) $S(1)$ transitions in the diffuse reflectance spectra of adsorbed H_2 in MOF-5 at loadings of one, two, four, and six molecules per $Zn_4O(O_2C-)_6$ cluster. The data were collected at 30 K. The band assignments are labeled according to their adsorption sites, primary (1°) or secondary (2°).

all of the $S(0)$ bands increase in intensity with time due to *ortho* to *para* conversion.

The $S(1)$ region shown in Fig. 7 is dominated by a band at 4676 cm^{-1} that displays a primary site concentration dependence. The other bands are weak, but we are able to confidently assign two of them to the primary site; there are potentially others. As expected, the $S(1)$ bands show a decrease in intensity with time due to *ortho* to *para* conversion. In general, the S bands are broader than those in the Q region with FWHMs ranging from 3 to 6 cm^{-1}. The principal S band frequencies are listed in Table I.

Rovibrational S bands should experience a redshift comparable to that of the pure vibrational Q bands. Additionally, the S bands are split due to the anisotropic nature of the interaction between H_2 and framework atoms. Since the $S(0)$ transition excites the singly degenerate $J=0$ level, any splitting in the $S(0)$ bands arises from the lifting of the degeneracy in $J=2$ levels. The results of simple density functional theory calculations (by using the commercial modeling package GAUSSIAN 03, with a 3-21G basis set), in which we mapped out the potential as a function of H_2 orientation, indicate that for the α site, both J and $|m|$ are still good quantum numbers with less than a 5% mixing of other sublevels. As shown in Fig. 1, we should expect to observe three $S(0)$ bands associated with the primary site. From the spectra in Fig. 6, we only note two such bands separated by 42 cm^{-1}. A third band may be unobservable below the noise of the spectra.

Predicting the relative strength of quadrupolar induced transitions is quite complex and involves a vector sum over the polarizability tensor of all the framework atoms.[53] For example, in solid H_2, the hexagonal closed packed symmetry leads to only $\Delta m=\pm 2$ transitions being allowed;[54] in contrast, a single polarizable entity displaced along the symmetry axis allows only $\Delta m=0$ and $\Delta m=\pm 1$ transitions with $\Delta m=0$ having 1/3 of the intensity of $\Delta m=\pm 1$.[55] In the case of the primary site, we expect all of the three transitions to be possible, with $\Delta m=\pm 2$ arising from the trigonal symmetry and $\Delta m=\pm 1,0$ arising from the lack of inversion symmetry. Predicting the relative contribution of the two terms requires knowledge of both the location and ionic polarizability of the framework atoms, which is beyond the scope of this paper.

In the case of the secondary binding sites, we observe at least four weaker $S(0)$ bands whose redshift and overall splitting is somewhat less than that of the primary site. The reduced splitting reflects the smaller interaction energies rather than a reduction in the symmetry of the sites.

For the $S(1)$ transitions, the picture shown in Fig. 1 is even more complicated since we are now probing excitations from a split $J=1$ level to a split $J=3$ level. In the case of the primary site, only the lower of the $J=1$ levels is expected to be populated at 30 K, so the number of $S(1)$ bands assigned in Fig. 7 reveals the splitting in the $J=3$ levels. If the lower $J=1$ state has $m=0$, then selection rules of $\Delta m=0,\pm 1,\pm 2$ should produce three distinct transitions consistent with the three definitive $S(1)$ bands, as shown in Fig. 7. The total splitting between the highest and the lowest frequency band is 59 cm^{-1}. There are no intense $S(1)$ bands associated with the secondary sites. This may be due to a decreased site symmetry, producing numerous transitions that lead to a washed out spectrum of multiple overlapping weak bands. At higher concentrations and lower temperatures, secondary site bands become observable, but these are still quite broad with FWHM in the range of 6–9 cm^{-1}.

Finally, we comment on the fact that both the $S(0)$ and $S(1)$ regions are dominated by a primary site band. From room temperature investigations of H_2 in rare gas mixtures, it has been established that S bands become more prominent with increasing polarizability of the perturbing atom.[56] Given the large intensities of the primary bands, it is concluded that H_2 is adsorbed near a region of large polarizability within the framework. Why the large intensity is limited to just one band is unclear but presumably reflects the detailed nature of the selection rules.

E. Orientational-vibrational bands

The spectral features arising from H_2 adsorbed on the primary site are significantly different from those associated with the secondary sites. The primary site produces the strongest S bands, blueshifted Q bands, and a very weak (unobservable) $Q(0)$ band. As per Sec. II and the discussion of Fig. 1, these three qualities suggest that the IR activation mechanism at this site is dominated by the H_2 quadrupole moment, inducing a dipole moment on the nearby MOF-5 atoms.

Orientational-vibrational transitions are those in which the J quantum number remains fixed but the orientational m quantum number changes. For the ground *ortho* state, this transition should occur at a higher frequency than the main $Q(1)$ band ($\Delta m=0$) that is permitted by both the isotropic and quadrupole mechanisms. Such a transition is evidenced by the band at 4194 cm^{-1} observed in Fig. 5, which is assigned as $Q(1)$ with $\Delta m=\pm 1$. This infers a 65 cm^{-1} splitting of the $J=1$ level for the primary site, which compares well with the proposed (but not observed) splitting of 58 cm^{-1} deduced from inelastic neutron scattering.[25] In fact, the agreement is almost ideal when one recognizes that the IR absorption bands reveal the splitting of the J levels in the

vibrationally excited state, which is expected to be about 10% greater than the splitting in the ground state. In principle, IR spectroscopy could also be used to observe the splitting in the ground state by first heating the sample to thermally populate the $J=1$, $m=\pm 1$ sublevels. A new band should appear ~ 60 cm^{-1} lower in frequency than the main $Q(1)$ band. We have observed this phenomenon for other samples,[51] but for MOF-5, the large splitting in the $J=1$ sublevels mandates such high temperatures that the bands become too broad to be observed.

F. Estimation of the site-specific adsorption energy

In practical terms, one of the most important goals of hydrogen storage research is the determination of the site-specific binding energies of promising adsorbents. To date, the principal experimental approach for MOFs is the isosteric analysis of H_2 adsorption isotherms, which were usually measured at 77 and 87 K, which yields a weighted-average adsorption energy as a function of coverage.[10,11,40,43] The extraction of accurate binding energies from an IR spectrum is challenging and requires a detailed understanding of the interactions; yet, with only a general knowledge of the framework material, it is possible to derive crude estimates of these energies from the vibrational redshifts of the different IR absorption bands.[36] In the absence of $H_2 \cdots H_2$ interactions, there are three dominant terms contributing to the interaction energy between H_2 and MOF-5,

$$V = V_{\text{disp}} + V_{\text{rep}} + V_{\text{elec}}, \tag{3}$$

where V_{disp} and V_{rep} are the traditional attractive and repulsive terms associated with the van der Waals interaction, and the additional V_{elec} term refers to the H_2 interaction with any ionic charges on the MOF-5 framework. This latter term contains the Coulombic interaction between the H_2 permanent quadrupole moment and framework charges, as well as the inductive term arising from MOF-5 dipoles, inducing a permanent dipole on the H_2.

The vibrationally excited state of H_2 has a 5% longer bond length than the ground state value and as such the magnitudes of all three interaction terms increase in the vibrationally excited state.[57,58] The change in the vibrational transition frequency is a tradeoff between (i) a redshift arising from the attractive part of the MOF-$5 \cdots H_2$ interaction and (ii) a blueshift arising from the repulsive part.[36] If the fractional increase was the same in each case, then there would be a simple relationship between the frequency shift and the site-specific binding energy. The repulsive term is the most difficult to model, but several authors have arrived at a general rule that it increases by about 8% in the vibrationally excited state.[36,58] Similarly, the H_2 polarizability and quadrupole moment are known to increase by 8% (Ref. 57) and 12%,[59] respectively. The partial charges on the MOF-5 framework were calculated by Sagara *et al.*[17] By combining all of this information, we can use the vibrational redshifts for the different sites to extract binding energy estimates of 4 kJ/mol for the primary site and 3 and 2.5 kJ/mol for the two observed secondary sites. The value for the primary site is consistent with the recently reported isosteric adsorption energies of approximately 3.8–5.2 kJ/mol.[10,11,40,43] Aside from the IR method, we are unaware of any other experimental technique used for determining site-specific binding energies. Theoretical predictions range from 2 to 7 kJ/mol for the highest binding site energy.[17,19,23,24] Yildirim and Hartman[13] predicted values for distinct sites that are clearly too high but claimed confidence in the relative values for the sites, estimating the binding energies of the secondary sites to be 65%–70% of the primary site.

V. SUMMARY

By using a uniquely designed sample chamber, the diffuse reflectance technique was applied to observe the IR-active rotational-vibrational transitions of the adsorbed H_2 in the microporous material MOF-5. At 30 K, there are sharp features that vary in intensity as a function of H_2 concentration and time; the latter results from slow *ortho* to *para* conversion. By monitoring these variations, bands have been assigned to specific Q and S transitions of molecules adsorbed on multiple framework sites, including the primary site identified in the previous experimental and theoretical reports. Hydrogen molecules at this primary site exhibit a center-of-mass translational mode frequency of 84 cm^{-1}, suggesting a substantial zero-point energy, which is at least 25% of the total binding energy. The application of simple theoretical considerations provides estimated site-specific binding energies of 2.5–4 kJ/mol from the observed vibrational redshifts. The frequencies of the rovibrational bands, while consistent with existing inelastic neutron scattering results, provide more information about rotational barriers at the different sites. This information will be invaluable for any detailed modeling of the anisotropic interactions between the H_2 and MOFs.

ACKNOWLEDGMENTS

We thank Orhan Talu and Asli Ertan for their assistance with the gas adsorption measurements and acknowledge the donors of the American Chemical Society Petroleum Research Fund and Research Corporation for their partial support of this research.

[1] M. Felderhoff, C. Weidenthaler, R. von Helmolt, and U. Eberle, Phys. Chem. Chem. Phys. **9**, 2643 (2007).
[2] S. Kitagawa, R. Kitaura, and S.-I. Noro, Angew. Chem., Int. Ed. **43**, 2334 (2004).
[3] G. Férey, Chem. Soc. Rev. **37**, 191 (2008).
[4] M. Dincă, A. Dailly, Y. Liu, C. M. Brown, D. A. Neumann, and J. R. Long, J. Am. Chem. Soc. **128**, 16876 (2006).
[5] H. Furukawa, M. A. Miller, and O. M. Yaghi, J. Mater. Chem. **17**, 3197 (2007).
[6] U.S. Department of Energy, Hydrogen, Fuel Cells & Infrastructure Technologies Program: Multi-Year Research, Development and Demonstration Plan, Sec. 3.3, 2007 (http://www1.eere.energy.gov/hydrogenandfuelcells/mypp/pdfs/storage.pdf).
[7] H. Li, M. Eddaoudi, M. O'Keeffe, and O. M. Yaghi, Nature (London) **402**, 276 (1999).
[8] M. Eddaoudi, J. Kim, N. Rosi, D. Vodak, J. Wachter, M. O'Keefe, and O. M. Yaghi, Science **295**, 469 (2002).
[9] J. L. C. Rowsell, Ph.D. thesis, University of Michigan, 2005.
[10] B. Panella, M. Hirscher, H. Pütter, and U. Müller, Adv. Funct. Mater. **16**, 520 (2006).
[11] A. Dailly, J. J. Vajo, and C. C. Ahn, J. Phys. Chem. B **110**, 1099 (2006).
[12] A. G. Wong-Foy, A. J. Matzger, and O. M. Yaghi, J. Am. Chem. Soc. **128**, 3494 (2006).
[13] T. Yildirim and M. R. Hartman, Phys. Rev. Lett. **95**, 215504 (2005).
[14] E. C. Spencer, J. A. K. Howard, G. J. McIntyre, J. L. C. Rowsell, and O. M. Yaghi, Chem. Commun. (Cambridge) 2006, 278.
[15] J. L. C. Rowsell, E. C. Spencer, J. Eckert, J. A. K. Howard, and O. M. Yaghi, Science **309**, 1350 (2005).
[16] O. Hübner, A. Glöss, M. Fichtner, and W. Klopper, J. Phys. Chem. A **108**, 3019 (2004).
[17] T. Sagara, J. Klassen, and E. Ganz, J. Chem. Phys. **121**, 12543 (2004).
[18] Q. Yang and C. Zhong, J. Phys. Chem. B **109**, 11862 (2005).
[19] F. M. Mulder, T. J. Dingemans, M. Wagemaker, and G. J. Kearley, Chem. Phys. **317**, 113 (2005).
[20] T. Sagara, J. Klassen, J. Ortony, and E. Ganz, J. Chem. Phys. **123**, 014701 (2005).
[21] T. Mueller and G. Ceder, J. Phys. Chem. B **109**, 17974 (2005).
[22] C. Buda and B. D. Dunietz, J. Phys. Chem. B **110**, 10479 (2006).
[23] F. Negri and N. Saendig, Theor. Chem. Acc. **118**, 149 (2007).
[24] E. Klontzas, A. Mavrandonakis, G. E. Froudakis, Y. Carissan, and W. Klopper, J. Phys. Chem. C **111**, 13635 (2007).
[25] J. L. C. Rowsell, J. Eckert, and O. M. Yaghi, J. Am. Chem. Soc. **127**, 14904 (2005).
[26] I. F. Silvera, Rev. Mod. Phys. **52**, 393 (1980).
[27] J. M. Nicol, J. Eckert, and J. Howard, J. Phys. Chem. **92**, 7117 (1988).
[28] J. Vitko and C. F. Coll, J. Chem. Phys. **69**, 2590 (1978).
[29] V. B. Kazansky, V. Yu. Borovkov, and H. G. Karge, J. Chem. Soc., Faraday Trans. **93**, 1843 (1997).
[30] S. S. Bragg, J. W. Brault, and W. H. Smith, Astrophys. J. **263**, 999 (1982).
[31] G. Herzberg, *Molecular Spectra and Molecular Structure, Spectra of Diatomic Molecules* (Kriegler, Malabar, Florida, 1989) Vol. I.
[32] G. Herzberg, *Infrared and Raman Spectra* (Van Nostrand, New York, 1996).
[33] J. van Kranendonk and H. P. Gush, Phys. Lett. **1**, 22 (1962).
[34] H. P. Gush, W. F. Hare, E. J. Allen, and H. L. Welsh, Can. J. Phys. **38**, 176 (1960).
[35] A. R. McKellar and M. J. Clouter, Can. J. Phys. **72**, 51 (1994).
[36] H. E. Hallam, *Vibrational Spectroscopy of Trapped Species* (Wiley, New York, 1973).
[37] T. Yildirim and A. B. Harris, Phys. Rev. B **66**, 214301 (2002).
[38] J. L. C. Rowsell, A. R. Millward, K. S. Park, and O. M. Yaghi, J. Am. Chem. Soc. **126**, 5666 (2004).
[39] S. A. FitzGerald, H. O. H. Churchill, P. M. Korngut, C. B. Simmons, and Y. E. Strangas, Rev. Sci. Instrum. **77**, 093110 (2006).
[40] J. L. C. Rowsell and O. M. Yaghi, J. Am. Chem. Soc. **128**, 1304 (2006).
[41] Methods for deriving apparent surface areas, pore volumes, and isosteric heats of absorption are described in F. Rouquerol, J. Rouquerol, and K. Sing, *Adsorption by Powders and Porous Solids* (Academic, London, 1999).
[42] J. Rouquerol, P. Llewellyn, and F. Rouquerol, Stud. Surf. Sci. Catal. **160**, 49 (2007).
[43] S. S. Kaye and J. R. Long, J. Am. Chem. Soc. **127**, 6506 (2005).
[44] B. Xiao, P. S. Wheatley, X. B. Zhao, A. J. Fletcher, S. Fox, A. G. Rossi, I. L. Megson, S. Bordiga, L. Regli, K. M. Thomas, and R. E. Morris, J. Am. Chem. Soc. **129**, 1203 (2007).
[45] L. M. Huang, H. T. Wang, J. X. Chen, Z. B. Wang, J. Y. Sun, D. Y. Zhao, and Y. S. Yan, Microporous Mesoporous Mater. **58**, 105 (2003).
[46] J. Hafizovic, M. Bjorgen, U. Olsbye, P. D. C. Dietzel, S. Bordiga, C. Prestipino, C. Lamberti, and K. P. Lillerud, J. Am. Chem. Soc. **129**, 3612 (2007).
[47] S. Bordiga, J. G. Vitillo, G. Ricchiardi, L. Regli, D. Cocina, A. Zecchina, B. Arstad, M. Bjorgen, J. Hafizovic, and K. P. Lillerud, J. Phys. Chem. B **109**, 18237 (2005).
[48] S. A. FitzGerald, S. Forth, and M. Rinkoski, Phys. Rev. B **65**, 140302(R) (2002).
[49] R. M. Herman and J. C. Lewis, Phys. Rev. B **73**, 155408 (2006).
[50] L. Xiao and D. F. Coker, J. Chem. Phys. **102**, 1107 (1995).
[51] S. A. FitzGerald, H. O. H. Churchill, P. M. Korngut, C. B. Simmons, and Y. E. Strangas, Phys. Rev. B **73**, 155409 (2006).
[52] S. Bordiga, L. Regli, F. Bonino, E. Groppo, C. Lamberti, B. Xiao, P. S. Wheatley, R. E. Morris, and A. Zecchina, Phys. Chem. Chem. Phys. **9**, 2676 (2007).
[53] J. D. Poll and J. van Kranendonk, Can. J. Phys. **39**, 189 (1961).
[54] V. F. Sears and J. van Kranendonk, Can. J. Phys. **42**, 980 (1964).
[55] F. R. Britton and M. F. Crawford, Can. J. Phys. **36**, 761 (1958).
[56] J. L. Hunt and H. L. Welsh, Can. J. Phys. **42**, 873 (1964).
[57] W. Kolos and L. Wolniewicz, J. Chem. Phys. **46**, 1426 (1967).
[58] A. V. Larin and E. Cohen De Lara, J. Chem. Phys. **101**, 8130 (1994).
[59] J. D. Poll and L. Wolniewicz, J. Chem. Phys. **68**, 3053 (1978).